

May 2017

# Fiber-based Stray Light Suppression in Spectrometers

Miaoxin Gong

---

Division of Combustion Physics  
Faculty of Science  
Lund University



Bachelor of Science Thesis



May 2017

# Fiber-based Stray Light Suppression in Spectrometers

Miaoxin Gong

Division of Combustion Physics  
Faculty of Science  
Lund University

Bachelor thesis supervised by  
Andreas Ehn, Elias Kristensson, Joakim Bood



**LUND**  
UNIVERSITY



## Abstract

Stray light is known as strong interference in spectroscopic measurements. With the creation of a novel kind of customized fibers, manufactured by the fiber optics group in Jena, Germany, a general experimental solution to this problem is possible. This thesis work is mainly aiming at testing and demonstrating how these fibers work for stray light suppression and their efficiency in measuring different types of optical signals. It is here demonstrated that the method is capable of stray-light suppression to more than one order of magnitude in Raman spectroscopy. In addition, studies of emission from Argon atoms show that the fiber is a good solution for suppression of background and high-frequency noises, which is reduced by more than a factor of 3 and 5, respectively. The results show that the method is feasible and efficient in practical use and that it has potential as a further tool in spectroscopy.

## Popular Abstract

Since the history of spectroscopy began with Isaac Newton's optics experiments, it has been beneficial to most research fields in natural science to study the interaction between matter and electromagnetic radiation. However, spectroscopy suffers from interferences called stray light. Stray light in an optical system can be described as light that deviates from the intended path and ends up in wrong places. In spectrometers, stray photons will distort the spectral characteristics of the detector. Therefore stray light can be a notable problem in spectroscopy, in particular when the spectral component of the signal-of-interest is near a strong spectral peak. The elimination or correction of stray light is desired in spectroscopic experiments.

A solution to this problem was developed in 2014 at the Division of Combustion Physics at Lund University. One potential development of this method could be to use special designed fibers. Such fibers were manufactured by Hatmut Bartelt's group in Jena, Germany, which is an active group in fiber-related research. This thesis work, which is done in collaboration with the fiber optics group, aims at testing and demonstrating how these fibers work for stray-light suppression and how well they can be applied in measuring different type of optical signals.

# Contents

<b>Abstract</b>	<b>i</b>
<b>Popular Abstract</b>	<b>ii</b>
<b>Glossary</b>	<b>iii</b>
<b>1 Introduction</b>	<b>1</b>
1.1 Motivation . . . . .	1
1.2 Why apply a fiber? . . . . .	3
1.2.1 Limitations of Using a Grid . . . . .	3
1.2.2 Advantages of Using a Fiber . . . . .	3
1.3 Stray light . . . . .	3
<b>2 Background Physics</b>	<b>4</b>
2.1 Atomic and Molecular Physics . . . . .	4
2.2 Laser Raman Spectroscopy . . . . .	5
<b>3 Experimental Equipment and Arrangement</b>	<b>6</b>
3.1 Experimental Equipment . . . . .	7
3.1.1 The Customized Fiber . . . . .	7
3.1.2 Spectrometer . . . . .	10
3.1.3 Detector(Camera) . . . . .	11
3.1.4 Light Sources . . . . .	12
3.2 Experiment Setup . . . . .	12
3.2.1 Testing Setup . . . . .	12
3.2.2 Raman Spectroscopy Setup . . . . .	13
<b>4 Analysis Method</b>	<b>14</b>
4.1 Spatial Lock-in Analysis . . . . .	14
4.2 Periodic Shadowing . . . . .	16
<b>5 Results</b>	<b>17</b>
5.1 Testings of the Fibers . . . . .	17
5.1.1 Imaging properties of the customized fibers . . . . .	17
5.1.2 Comparison between different imaging magnifications . . . . .	20
5.2 A Demonstration of Fiber-based PS Technique in Emission . . . . .	22
5.3 Fiber-based Laser Raman Spectroscopy . . . . .	24
<b>6 Conclusion</b>	<b>25</b>
<b>7 Outlook</b>	<b>25</b>
<b>Acknowledgement</b>	<b>25</b>

<b>References</b>	<b>26</b>
<b>Appendix A Parameters of the Customized Fibers (from the manufacturing research group)</b>	<b>28</b>
<b>Appendix B More sketches of Experimental Setup</b>	<b>32</b>



## **Glossary**

**CCD** Charged-coupled Device. 11

**EMCCD** Electron Multiplying CCD Camera. 12

**NA** Numerical Aperture. 9

**ND** Neutral Density. 13

**PS** Periodic Shadowing. 1

**SNR** Signal-to-noise Ratio. 3

# 1 Introduction

## 1.1 Motivation

A large number of research fields in natural science benefit from optical spectroscopy since it is widely applicable for e.g. classification of stars, space exploration, and identification of molecular structures [1]. However, it is well known that spectroscopic measurements suffer from interferences called stray light, causing spectral distortion that reduces measurement accuracy [2]. Stray light in an optical system can be described as light that deviates from the intended path and hence ends up in the wrong place [3]. In spectrometers, where light is spectrally dispersed at the detector, stray photons will thus distort the spectral characteristics of the detected light. Therefore stray light could be a notable problem when the spectral component of the signal-of-interest is near a strong spectral peak. In severe situations, stray light may even conceal the presence of spectral lines. A well-known example of such a situation is Raman spectroscopy where the signal-of-interest is very weak compared to the elastic scattering of the laser light. Moreover, the spectral shift between the laser light and the Raman signal is sometimes very small since it is determined by the separation between vibrational and rotational energy levels in the molecule. Therefore, the elimination or correction of stray light is desired and sometimes a necessity in spectroscopic experiments.

Multiple effects may factor in the origins of stray light. Existing methods for stray light correction are based on both optical solutions and by using computer-aided approaches. Using double or triple monochromators can mitigate stray light distortions, but these are costly and time-consuming solutions since they are based on a scanning procedure, which also leaves out the possibility of acquiring instantaneous 2D spectra. The need to monitor and compensate for variation in the brightness of the object in all scanning instruments leads to a common complication with such methods. During the detection process, high-performance holographic notch filters are often used to inhibit the detection of stray light caused by a specific source. Both these experimental methods are limited in their number of applications. As for the computer-aided approaches, the derivative method is probably the most wellknown. The derivative method extracts and analyzes derivatives of the spectrum and the benefit is that broad spectral structures are suppressed relative to sharper bands to allow the identification of relatively weak features. However, derivatives are extremely sensitive to noise and their heavy reliance on smoothing deteriorates spectral resolution. Also, fine-tuning is required in obtaining optimum results for a given line width, which is not applicable when the spectrum contains lines with variations in bandwidth.

A solution to this problem was developed in 2014 at the Division of Combustion Physics at Lund University [4]. This novel general method was presented and named Periodic Shadowing (PS) and it proved to enable effective stray light elimination in spectroscopy in a wide range of applications. The fundamental idea of PS is mainly based on lock-in amplification [5][6]. It strongly reduces the stray light problem by tagging the photons that enter the spectrometer with a predefined pattern. The configuration presented in Ref.[4] utilized a Ronchi (square wave) grid target mounted at the entrance slit to tag the

light (as shown in Fig.1). In this way, no other optical modification to the spectroscopic system is required. Because the entrance slit is imaged onto the detector for a range of wavelengths, the fine stripes of the Ronchi grid will effectively cast periodic shadows with a given spatial frequency and phase (along the slit direction), superimposed on all spectral features. The stray light does not maintain this well-defined structure during its passage through the spectrograph and will, in contrast to the signal photons, appear as a wavelength-dependent intensity offset at the detector. This distinction allows the signal photons to be identified and separated from the stray light, both in one- and two-dimensional measurements, using a simple post-processing routine. A lock-in detection algorithm [5] is incorporated on each column of the acquired spectrum to extract only the information that appears with the same periodicity as that of the Ronchi grid. Apart from suppressing stray light, this approach also has the added benefit of reducing the impact of white random noise. Furthermore, with the tagging process and data acquisition occurring simultaneously, pre-calibrations and blank or background recordings are avoided.

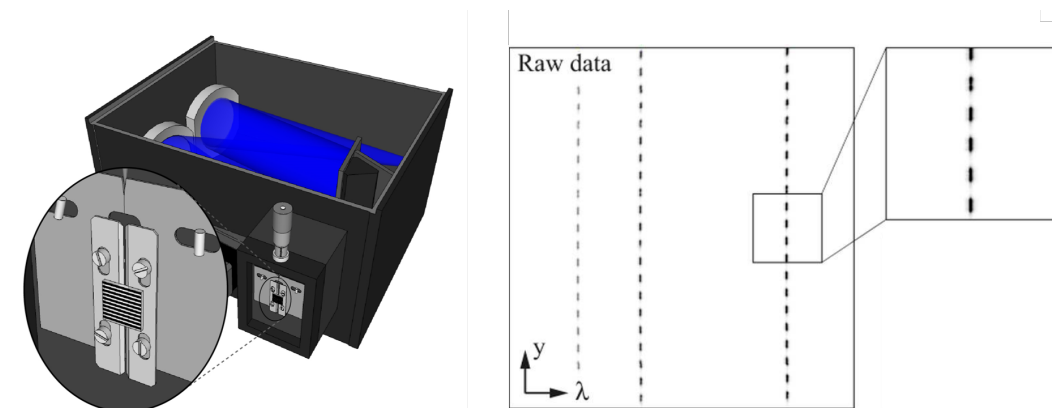


Figure 1: Left: the sketch of a PS spectrometer with Ronchi grid. Right: raw PS image of an cadmium emission lamp in which a spatial modulation of the spectral lines created by the grid [4, 7].

One potential development of this method could be to use specially designed fibers. Such fibers were manufactured by Hartmut Bartelt's group in Jena, Germany, which is an active group in fiber-related research. The customized fiber has 19 capillary fibers inside and features as having circular structure on one end (collection side) and line structure on the other end (output side). On the circular side and line side, the capillary fibers are respectively arranged in a bundle and in a linear row. As the light is transmitted into the collection side, it transmits through the capillary fibers and emerges into an even, linear pattern which can be used in the PS method as a predefined unique pattern. The tagging process performed by the fiber has, in principle, no light loss compared to the Ronchi grid. Thus, a feasibility study on applying the customized fibers is needed and valuable.

The project, which is done in collaboration with the fiber optics group in Jena, aims at testing and demonstrating how these fibers work for stray light rejection and how well they can be applied in measuring different types of optical signals. If the method proves

to be feasible, this efficient, experimental and convenient approach to suppress stray light in optical spectroscopy will have great potential to be popularized.

## **1.2 Why apply a fiber?**

### **1.2.1 Limitations of Using a Grid**

One drawback with the PS method concerns the loss of signal due to the usage of the Ronchi grid, which reflects 50% of the incident light to the spectrometer – a characteristic that will negatively affect the signal-to-noise ratio (SNR) of a PS spectrometer[7]. In Ref.[4], Kristensson et al. investigated how the signal-to-noise differed between an ordinary spectrometer and one based on the PS method. The a priori characteristics of the signal of interest – its unique spatial phase and frequency – can be exploited to reduce noise. Two processes are mainly responsible for the filtering of noise. A (spatial) band-pass filter is applied on the signal, removing redundant spatial frequencies that otherwise add noise. Though it can be compensated in terms of SNR by the approach above, the loss of light introduced by the Ronchi grid still can be a problem to the PS method.

### **1.2.2 Advantages of Using a Fiber**

The first advantage of using a fiber is that light loss will be significantly reduced in comparing to the Ronchi grid. Functionally, the customized fiber provides a pre-defined periodic pattern as the grid does. The transmission efficiency is nearly 100% inside the fiber. In principle, the 50% reflection by using a grid will drop down to none. This property allows the measuring system to receive and process signal about twice weaker than when a grid is applied.

The second advantage is that using a fiber allows more flexibility in the optical system. When using a grid, the experiment setup can only be fixed in position in order to insert the signal light from the transmitting end (light source) to the receiving end (spectrometer and detector/camera). In many cases which involve a laser as light source, this can cause inconvenience and limitations while building up the experiment setup. The light source needs to be inserted into the detection slit, but shooting a laser beam directly towards a detector would certainly damage the camera. To avoid this, more optical components such as mirrors or lenses need to be introduced in to the system, which increase the difficulty during alignment. However, the transmission medium made up from a fiber provides the possibility the for experimenter to prepare independent light source system and detection system. In the present experiment, where the light source system and detection system were built independently, this advantage was clearly reflected.

## **1.3 Stray light**

Stray light lacks a strict definition as well as a conclusive and general solution at the moment. As mentioned in 1.1, stray light can be described as an optical phenomenon that comprises all spurious light arriving the detector in unintended ways, manifesting itself

as background enhancements that vary across the wavelength range of the spectrum [4]. One of the common definitions is that it is the ratio of spurious radiation to the primary or desired radiation [8]. Since stray light can be defined as a ratio, either the numerator or the denominator affects it. Stray light can be decreased by increasing ratio of primary radiation intensity to spurious radiation intensity.

Sources of stray light are from multiple effects. Origins such as imperfections in optical components and strong radiation line wing overlap are often reported. In a spectrometer, light scattered at an imperfect or unclean surfaces is usually the chief source of stray light in a monochromator. Also, there are many effects causing stray light distortion, including deterioration detection limits, deviation analysis, weak spectral feature concealment, resolution loss and calibration error [3]. Specifically, stray light in spectrometers appears as undispersed light superposed on the monochromatic radiation. Anything that causes the light passage to deviate from the direct path, such as repeated reflexions, light scattering from imperfection or dust in the polished surfaces of the optical components, edges of diaphragms, can contribute to the source of stray light in a spectrograph systems [3].

## 2 Background Physics

This section provides a brief overview of atomic physics, molecular physics and laser Raman spectroscopy concerning this experiment.

### 2.1 Atomic and Molecular Physics

In physics, an atom emits a photon as a result of a transition from a higher to a lower electronic energy state. The energy of the emitted photon is given by the formula:

$$E_{\text{photon}} = h\nu \quad (2.1)$$

where  $h$  is Planck's constant,  $\nu$  is the frequency. The spectrum of the electromagnetic radiation that is emitted by a number of specific atoms is a result of transitions between several quantum states. Therefore, the information of the energy structure of an atom can be obtained and studied by the emission spectrum. On the other hand, the internal energy of a molecule is distributed from not only among the electronic states, but also between vibrational and rotational states. The structure of a molecule can be obtained by interactions between molecules and photons in designed laser experiments. In quantum mechanics, the Hamiltonian  $\hat{H}$  is an observable of the molecular energy correlated with the total energy operator.

Diatomic molecules are the simplest types of molecules and serve here as an example for a discussion of the energy structure of molecules. The Hamiltonian describing the molecular energy of a diatomic molecule can be expressed as:

$$\hat{H} = \hat{T}^N(R, \theta, \phi) + \hat{T}^e(r) + \hat{V}(r, R) \quad (2.2)$$

where  $\hat{T}^N$  is the kinetic energy of the nuclei,  $\hat{T}^e$  is the electron kinetic energy and  $\hat{V}$  is the electrostatic potential energy of the electrons and the nuclei.  $R$  and  $r$  are the spatial parameters of internuclear distance and the coordinates of the electrons.  $\theta$  and  $\phi$  are the rotational angles of the internuclear axis. According to the assumption of the Born–Oppenheimer approximation, the motion of electrons and nuclei can be separated in a molecule. So the three independent energy contributions in Eq. 2.2 can be solved separately to calculate the eigen values to the Hamiltonian. The energy structure of more complex molecules is far more demanding to model. For instance, naphthalene ( $C_{10}H_8$ ), the sample used in this thesis, has rather a complex molecular structure. Rotational energies, however, can be disregarded here since merely samples in solid phase are considered. A schematic of the naphthalene structure is displayed in Fig. 2[9] where the vibrational modes are included.

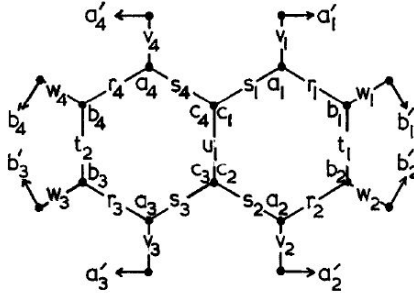


Figure 2: Valence co-ordinates for naphthalene [9].

## 2.2 Laser Raman Spectroscopy

Raman spectroscopy is a powerful tool for the investigation of molecular vibrations and rotations [10]. The introduction of lasers has made significant improvement to this conventional spectroscopy approach. In the present experiment, solid Naphthalene was used due to its relatively large Raman scattering cross section.

Rayleigh scattering is an example of elastic scattering, where the frequency  $\omega$  (wavelength  $\lambda$ ) of the Rayleigh scattered light is the same as that of the incoming electromagnetic radiation (Fig. 3). Raman scattering may be regarded as an inelastic collision of an incident photon  $\hbar\omega_i$  with a molecule in the initial energy level  $E_i$ . Following the collision, a photon  $\hbar\omega_s$  with lower energy is detected and the molecule is found in a higher energy level  $E_f$ :

$$\hbar\omega_i + M(E_i) \rightarrow M^*(E_f) + \hbar\omega_s, \text{ with } \hbar(\omega_i - \omega_s) = E_f - E_i > 0. \quad (2.3)$$

The inelastically scattered photon will be shifted to a lower frequency for the total energy of the system to remain balanced. This inelastically scattered photon is called *Stokes radiation*.

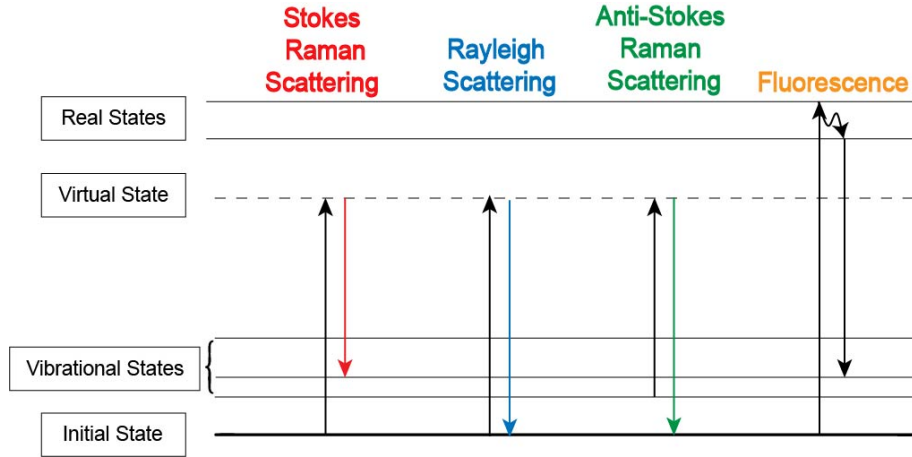


Figure 3: Energy-level diagram showing the states involved in Raman spectra.

The energy difference  $\Delta E = E_f - E_i$  may appear as vibrational, rotational or electronic energy of the molecule. If the photon  $\hbar\omega_i$  is scattered by a vibrationally excited molecule, it may gain energy and the scattered photon has a higher frequency  $\omega_{as}$  where

$$\hbar\omega_{as} = \hbar\omega_i + E_i - E_f, \text{ with } E_i > E_f. \quad (2.4)$$

This photon scattering is called *anti-Stokes radiation*.

In the energy-level scheme shown in Fig. 3, the intermediate state  $E_v = E_i + \hbar\omega_i$  of the system "during" the scattering process is often formally described as a *virtual state* which is not a "real" stationary eigenstate of the molecule.

The scattering cross sections in spontaneous Raman scattering are very small, typically on the order of  $10^{-30} \text{cm}^2$ . As a result, the main difficulty of Raman spectroscopy is separating the weak inelastically scattered light from the intense Rayleigh scattered laser light. The stray light from the intense laser line conceals the Raman spectral features, where, in principle, the PS method is applicable for eliminating stray light. Therefore, laser Raman spectroscopy is suitable to experimentally verify the capability of the PS technique realized with the customized fiber.

### 3 Experimental Equipment and Arrangement

The first part of this section will describe parameters and characteristics of the equipment mainly employed in the thesis work. The second part will describe the experimental setup that was used in this project as well as considerations of the experiments design.

## 3.1 Experimental Equipment

### 3.1.1 The Customized Fiber

The three customized fiber bundles that are investigated in this work were manufactured by Hartmut Bartelt's group in Jena, Germany, which is an active group in fiber-related research.

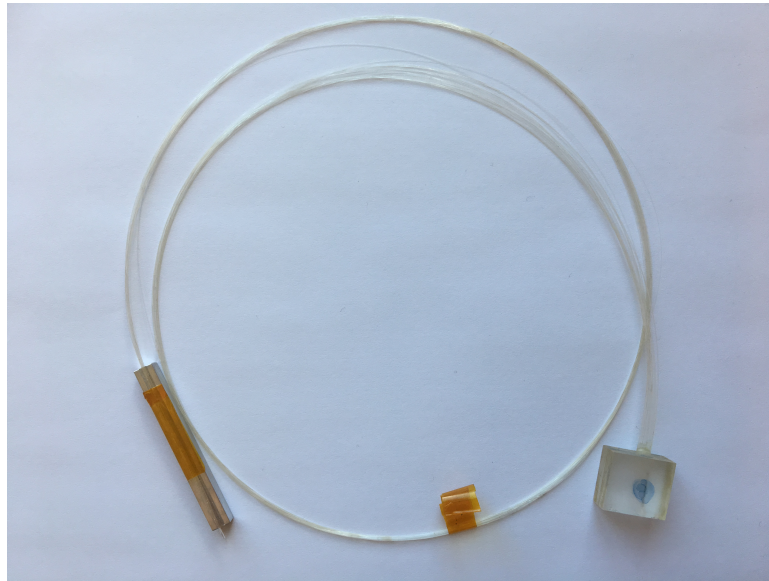


*Figure 4: Photograph of one of the customized fibers (Tag: "Ehn-2").*

### Basic Structure

As the protagonist of the experiment, the customized fibers (Fig. 4) need to be studied thoroughly to determine its properties and performance. The customized fiber bundle consists of 19 optical fibers that are arranged in a circular structure on one end (collection side) and a line structure on the other end (output side). The length of the fibers varies in the range 0.5-1.0m. In Fig. 5 and Fig. 6 the structure of collection end and output end is shown respectively.

The 19 fibers are arranged as a bundle on the collection end where they are fixed in a capillary. To match the fiber bundle, the cover capillary has an inner and outer diameter of  $1294\mu\text{m}$  and  $1610\mu\text{m}$ , respectively. The fibers are arranged in a linear row at the output end, each fiber separated with a distance to achieve a reproducible periodic intensity modulation pattern at the fiber output. The distance between each active fiber ("guidance fiber") is created using a piece of a dummy fiber ("distance fiber") that is not connected to the fiber inlet and hence, does not direct any light. All these 37 fibers, whereof only 19 direct light, are fixed in a microscope plate holder. The corresponding arrangement of both ends is as followed:



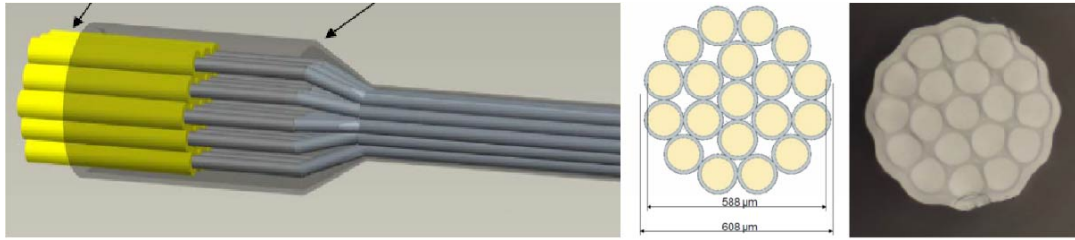


Figure 5: Schematic diagram and real image of the collection end ( $19\times$  circular structure).

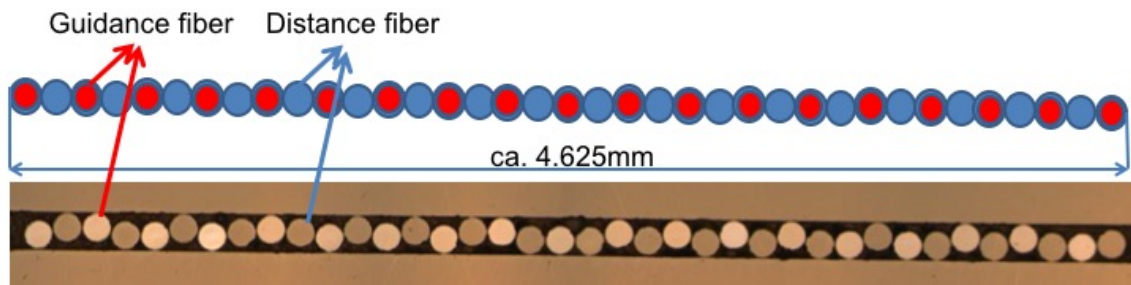


Figure 6: Schematic diagram and real image of the output end ( $37(19)\times$  row). The red circles represent the "guidance fiber" and the blue ones represent the "distance fiber".

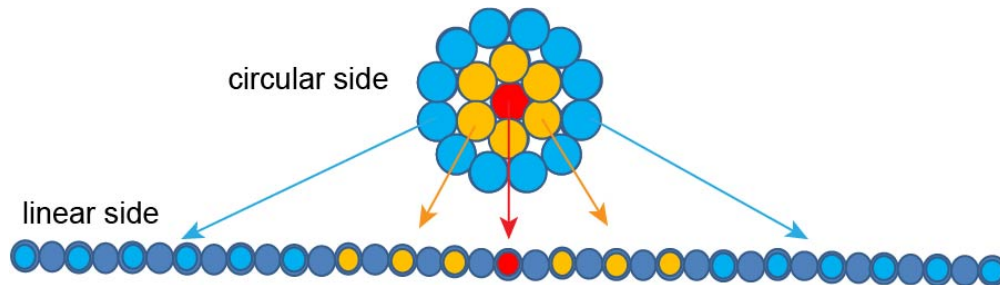


Figure 7: Scheme of the circular and linear ends of the customized fiber bundle. The different optical fibers are color coded for identification.

- The central fiber of the bundle is put in the middle of the linear arrangement;
- The surrounding 6 fibers of the bundle are put next to the first (central) fiber (3 on each side);
- The remaining 12 fibers of the bundle in the outer ring are put on the outside of the linear arrangement (6 on each side);

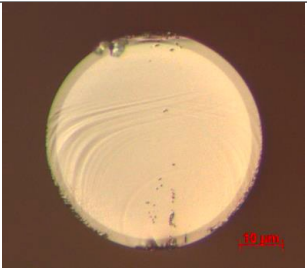
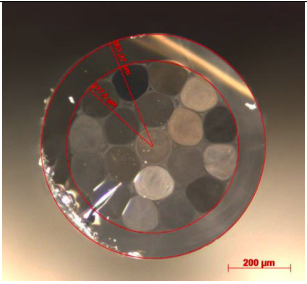
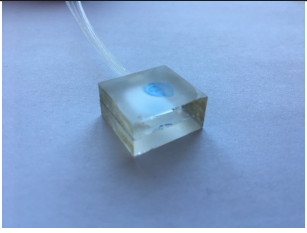
\* between 2 guidance fibers lies a "distance fiber".

With the gap generated by the "distance" fibers between every two capillary fibers, a unique pattern of light can be created. When the light inserts into the circular end, it transmits through the capillary fibers and emerges into an even, linear pattern. A predefined tagging is produced through this process as a modulation onto the inserting light, which is suitable for PS.

## Important Features

Due to the fact that these fibers were manufactured by hand, they are not exactly identical. Though basic features as material, dimensions were informed by the manufacturing group (as seen in Tab.1), still, other important optical features such as Numerical Aperture (NA), transverse mode etc. need to be acquired by experiments. Further testings are reported in section 5.1 to determine their individual differences and optical performance.

*Table 1: General dimensions of the fibers measured by the manufacturing group.*

	Approximate dimensions	Photograph
Fiber	Fiber core diameter: $114\mu m$ ; Cladding diameter: $126\mu m$ ; Coating diameter: $230\mu m$	
Capillary for collection end	Outer diameter: $\sim 1610\mu m$ Inner diameter: $\sim 1294\mu m$	
Holder for output end	LWH: $2.0 \times 1.0 \times 0.5cm$	

**Multi-mode Fiber** The single fibers inside the customized fibers are multi-mode fibers, which have a fairly large core diameter that enables multiple light modes propagation.

**NA in Fiber optics** A multi-mode optical fiber will only propagate light that enters the fiber within a certain cone, known as the acceptance cone of the fiber. This acceptance cone can be used to experimentally describe the NA in fibers.

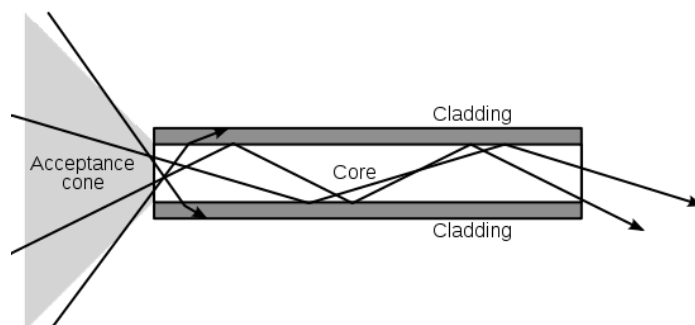


Figure 8: Schematic diagram of light propagation through a multi-mode optical fiber [11].

### 3.1.2 Spectrometer

The spectrometer used in the experiment is the Andor Shamrock SR-303i (shown in Fig. 9), which is a automated high throughput flat field imaging spectrograph with triple grating turret [12]. It is a Czerny-Turner type spectrometer. The core part is a planar linear grating. The incident light enters from the input slit and it is focused onto the grating by the concave mirror. Then the light is deflected by another concave mirror and focused onto the CCD detector at the exit to detect the intensity of light. Tab.2 shows the summary of specification of the spectrograph.

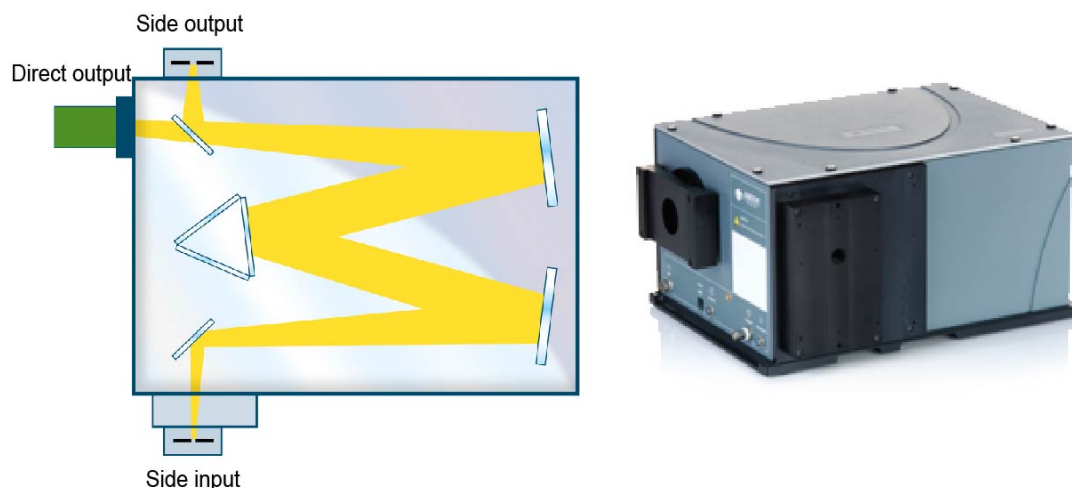


Figure 9: The scheme and photo of the Andor Shamrock SR-303i Spectrometer [12].

**Features and Specification** The Andor Shamrock SR-303i Spectrometer has some features and benefits from them, such as [12]:

- Pre-aligned, pre-calibrated;
- Image astigmatism correction;
- Motorized, indexed triple grating turret to be upgradable in-the-field;
- High resolution in space.

Table 2: Specification summary of the Andor Shamrock SR-303i spectrometer[12].

Aperture	F/4
Focal length	303 mm
Gratings	Interchangeable indexed triple turret Grating 1: 600 l/nm Grating 2: 1200 l/nm Grating 3: 1800l/nm
Slit width range (input/output)	Motorized 10 $\mu\text{m}$ to 2.5mm Wide aperture option to 12 mm
Communication	USB 2.0
Wavelength accuracy	0.04 nm
Wavelength repeatability	4 pm
Stray light	$2.2 \times 10^{-5}$

### 3.1.3 Detector(Camera)

The detector/camera used in this work is Andor Luca R604 [13] (shown in Fig.10).

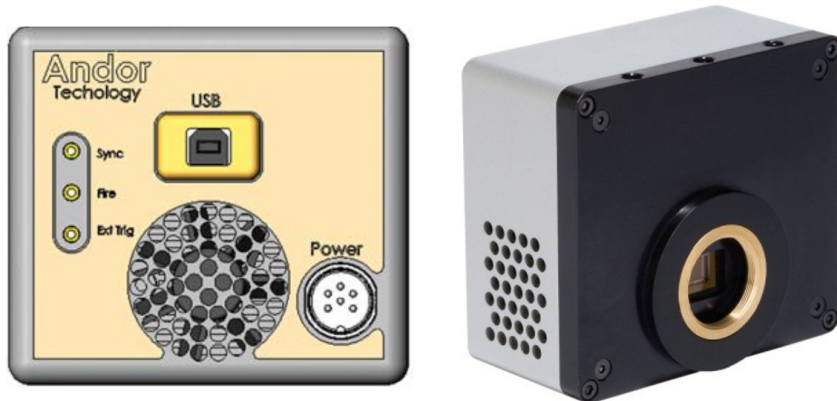


Figure 10: The scheme and photo of the Andor Luca R604 EMCCD [13] Camera.

A Charge Coupled Device (CCD) is a device for the movement of electrical charge, with an integrated circuit etched onto a silicon surface. Photons incident on this surface

generate charge that can be read by electronics and turned into a digital copy of the light patterns falling on the device. CCD as a spectrometer detector has many advantages. An Electron Multiplying CCD Camera (EMCCD) is an image sensor with sensitivity that operates at high speed by amplifying the charge signal before the charge amplifier. The readout noise is effectively by-passed by amplifying the signal and readout noise no longer limits the sensitivity.

### 3.1.4 Light Sources

**Emission Lamp** An Argon discharge lamp was used as light source in the first half of the experiment. The spectral region 665-835 nm was used and observed in the experiments.

**Laser** The laser was a continuous source with center wavelength of 405 nm, peak width of about 5 nm (estimated by FMHW of Raman peaks), spot size of about  $0.5 \times 0.8$  mm and power of about 300 mW.

## 3.2 Experiment Setup

The setup has been modified several times to improve the performance of the experiment. It can be divided into three parts involving the light source system, focusing system and detection system. During the testing section, an Argon lamp was used as light source in order to refine optical layout in the focusing system and detection system (3.2.1). After approaching the best optical condition for the measuring system, the laser was introduced to perform laser Raman spectroscopy (3.2.2).

### 3.2.1 Testing Setup

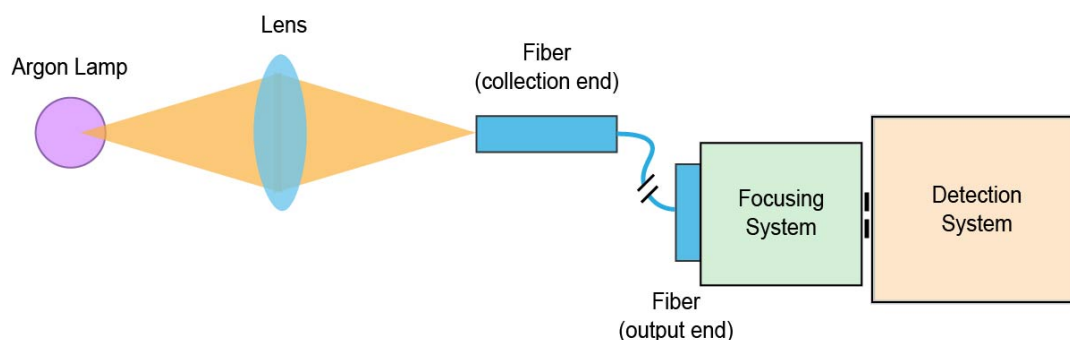


Figure 11: Sketch of the testing setup (for testing the focusing system and detection system).

During the testings, light from an Argon spectral lamp was collected and focused onto the collection end of the fiber. In the early testings, the output end of the fiber was directly mounted in front of the entrance slit. Then in the later stage, a focusing system was introduced (including lens, aperture, optical bench etc.), which is displayed in Fig. 27.

Multiple parameters were tested to achieve ideal imaging condition. This is described in detail in section 5.1.

Additionally, since there was no standard mounting between the camera and the spectrometer, a homemade level platform was employed to adjust the relative position among them, as seen in appendix B.

### 3.2.2 Raman Spectroscopy Setup

As shown in Fig. 12 and 13, a continuous laser beam was generated and propagated through a Neutral density (ND) filter (which only reduces the amount of light passing through without changing the color of the laser light). Then the filtered laser light was directed to the Raman sample (naphthalene). The Raman scattering signal is generated by the sample when exposed to the laser. The light source system mentioned above was fully covered by black cardboard shield for the safety concerns. Then the Raman signal was collected by a 200mm spherical lens and filtered by an aperture mounted right after the lens, whereafter it was focused onto the collection end of the fiber. The signal light was transmitted through the optical fibers in the fiber bundle. After reaching the output end, the signal from the fiber array (the output end of the fiber) was refocused onto the entrance slit of the spectrometer. The signal light was then transmitted through the optical fibers in the fiber bundle. After reaching the output end, the signal from the fiber array (the output end of the fiber) was refocused onto the entrance slit of the spectrometer (slit width:  $20\mu\text{m}$ ).

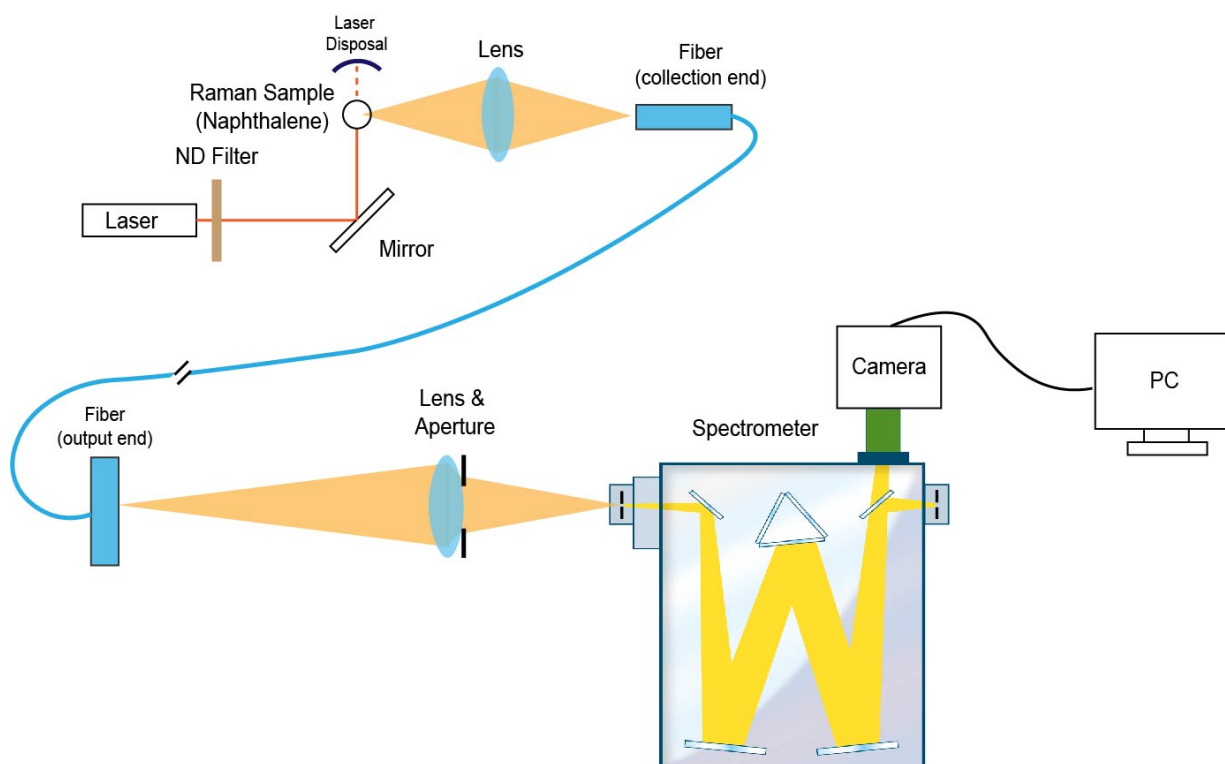


Figure 12: Sketch of the experiment setup (for Raman spectroscopy).

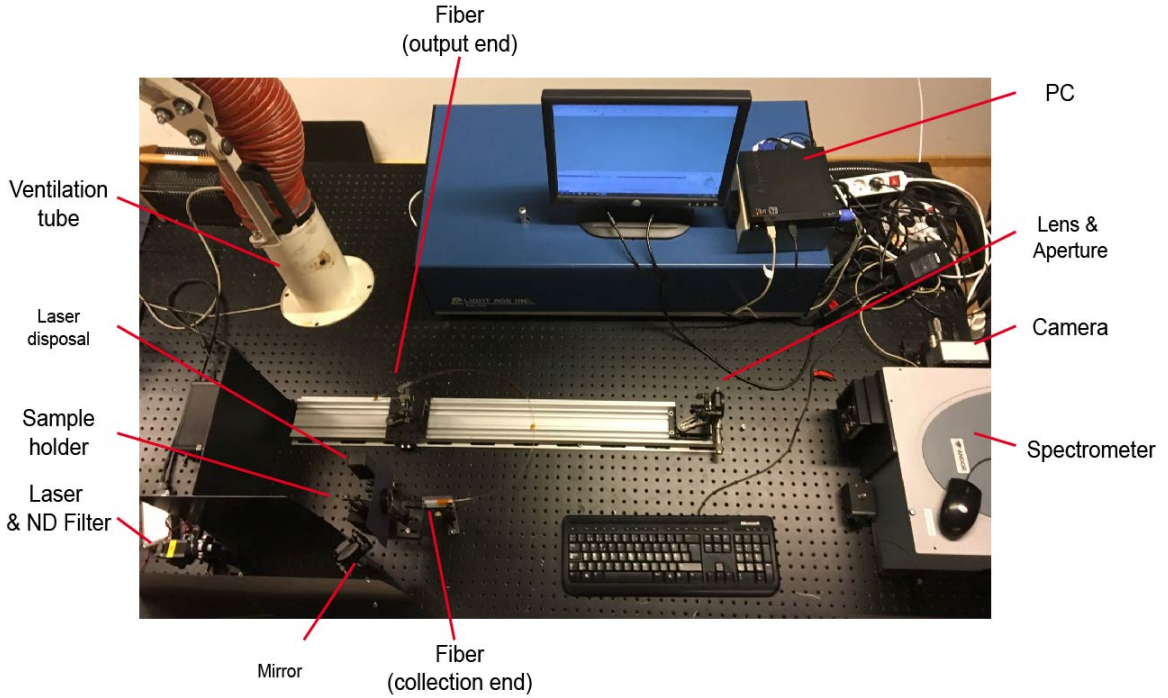


Figure 13: Photo of the experiment setup (for Raman spectroscopy).

The image was finally captured by the camera and processed by the PC. Additionally, different exposure time was set nearly saturated according to different imaging conditions and every spectrum was averaged by multiple measurements.

## 4 Analysis Method

This section gives a brief introduction to the analysis method of stray light suppression used in the thesis work.

### 4.1 Spatial Lock-in Analysis

Lock-in analysis is a type of signal amplifier that can extract a signal with a known carrier wave from a noisy environment. It is usually used for signals periodically changing over time but in principle also works for signals with spatial modulated components.

Consider a column in a modulated spectrum ( $I$ ) at the wavelength  $\lambda$  that contains a spectral line:

$$I(\lambda, y) = A_\lambda(y) \sin(2\pi\nu_g y + \phi_\lambda(y)) + B_\lambda(y) \quad (4.5)$$

where  $\nu_g$  is the modulation frequency of the grating,  $y$  is spatial vector,  $A$  is the amplitude of the modulated signal,  $B$  is a non-modulated background,  $\phi_\lambda(y)$  is the unknown

spatial phase of the superimposed modulation. The lock-in algorithm is to extract  $A$  (where the signal resides in) and reject  $B$  (contains stray light).

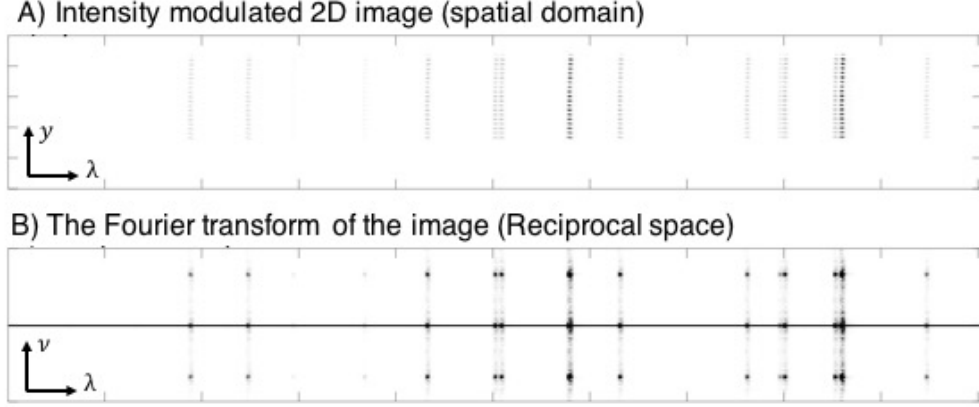


Figure 14: Intensity modulated 2D spectrum with a spatial modulation of the spectral lines along the vertical direction. A) The example is an emission spectrum from an Argon lamp transmitted by the customized fiber to the spectrometer and detected by the CCD camera; B) the Fourier transform of the image shows how the spectral information is transferred away from the first order spatial frequency.

First, by Eq. 4.6 and 4.7, two reference signals,  $I_{r_1}$  and  $I_{r_2}$  are defined, which share the same periodicity ( $\nu_g$ ) as the modulated spectrum, but are phase-shifted  $\pi/2$  radians.

$$I_{r_1} = \sin(2\pi\nu_g y) \quad (4.6)$$

$$I_{r_2} = \cos(2\pi\nu_g y) \quad (4.7)$$

The following expressions are given by and simplified from multiplying the reference vectors with the column vector  $I(\lambda, y)$ :

$$I_\lambda^1 = \frac{1}{2}A_\lambda(\cos(\phi_\lambda(y)) - \cos(4\pi\nu_g y + \phi_\lambda(y))) + B_\lambda \sin(2\pi\nu_g y) \quad (4.8)$$

$$I_\lambda^2 = \frac{1}{2}A_\lambda(\sin(\phi_\lambda(y)) + \sin(4\pi\nu_g y + \phi_\lambda(y))) + B_\lambda \cos(2\pi\nu_g y) \quad (4.9)$$

When applying a low-pass filter with a cut-off frequency of  $\nu_{cut} \leq \nu_g$  on Eq. 4.8 and 4.9, all components are removed except from the first component (the DC component):

$$\tilde{I}_\lambda^1 = \frac{1}{2}\tilde{A}_\lambda \cos(\phi_\lambda(y)) \quad (4.10)$$

$$\tilde{I}_\lambda^2 = \frac{1}{2}\tilde{A}_\lambda \sin(\phi_\lambda(y)) \quad (4.11)$$



where the tilde assignment marks are applied frequency filtering. Therefore, extracting  $\tilde{A}_\lambda$  is expressed as:

$$\tilde{A}_\lambda = 2\sqrt{\left(\tilde{I}_\lambda^1\right)^2 + \left(\tilde{I}_\lambda^2\right)^2} \quad (4.12)$$

The function of low-pass filter used above is seen as:

$$U_\nu = e^{\left(-\frac{\nu}{\nu_{cut}}\right)^8} \quad (4.13)$$

## 4.2 Periodic Shadowing

Inspired by the (spatial) lock-in amplification [5, 14], the PS method was proposed and demonstrated as a technique to effectively suppress stray light in spectroscopic equipment. Essentially, it requires spatially modulated light at the entrance slit of the spectrometer. To achieve this, a Ronchi grid (transmission grating) mounted at the entrance slit was performed in previous works [4, 14]. In this work, however, the customized fiber is used instead of the Ronchi grid to create the spatial modulation of the spectral lines.

When the light transmits through the spectrometer, some photons will be deflected because of the imperfection and uncleanness in the spectrometer and the optics, forming the stray light. However, the photons traveling in the correct path, which are the signal photons, maintain the modulation information with a spatial distribution set by the output end of the fiber and end up at the detector plane. This different characteristic between stray light and signal light provide the possibility to apply the spatial lock-in analysis presented in 4.1. Fig. 14 shows a 2D spectrum acquired with the customized fiber, and its modulated pattern superimposed on the spectral lines is clearly visible.

The following Fig. 15 illustrates how the information is extracted by the PS method. A intensity modulated 2D spectrum of an Argon emission lamp is shown in Fig. 15(a). After column-by-column Fourier transform, each column is multiplied with two reference signals having a relative phase shift of 90 degrees (Eq. 4.6 and Eq. 4.7). In this way, the modulated component is transformed into a DC component. Thus, a low-pass filter is able to be applied to extract the information. The multiplication with the reference signals transfers the stray light at low frequencies into higher frequencies so that it can be removed by the low-pass filter. The inverse Fourier transform of the filtered data is then extracted to generate a spectrum with strongly reduced stray light component, as shown in Fig. 15(b).

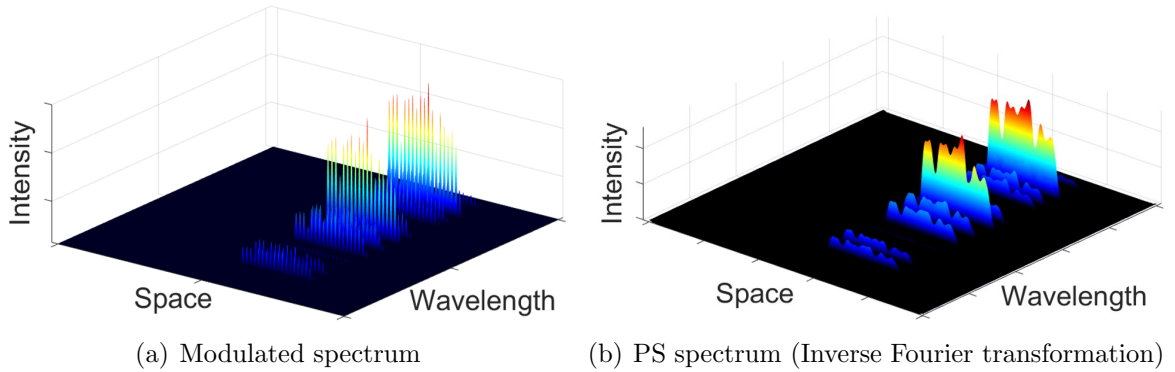


Figure 15: An example of the PS analysis on an Argon emission spectrum.

## 5 Results

This section, presenting experimental results and corresponding discussions, is divided into three parts. First, comparative tests are performed to determine the optical properties of the customized fibers. Also, parameters including imaging magnifications, opening size of the aperture, slit width and acquisition time, were tested to attain the ideal imaging condition. Second, emission was studied with the fiber-based PS method. Third, fiber-based Laser Raman Spectroscopy is performed.

### 5.1 Testings of the Fibers

#### 5.1.1 Imaging properties of the customized fibers

**Individuality of the customized fibers** Since the customized fibers were manufactured by hand, individual differences are inevitable. Testings are done to check the consistency of these fibers. At first, three customized fibers (tagged respectively: “Ehn-2”, “Ehn-4”, “Ehn-5”) were sent by the research group from Jena, Germany. Unfortunately, one of the fibers tagged “Ehn-2” was damaged for some reason before the experiment started. So the following testing results are based on the other two, “Ehn-4” and “Ehn-5”.

The setup shown in Fig. 27 was used for this test. In this testing, the fibers were mounted in front of the entrance slit without any focusing optics and the acquisition setup of the camera maintained the same. Hence the result displays the original imaging features of the fibers. Fig. 16 shows the raw image comparison between the two customized fibers “Ehn-4” and “Ehn-5”. Fig. 17 shows both the raw and PS spectra comparison between the two fibers.

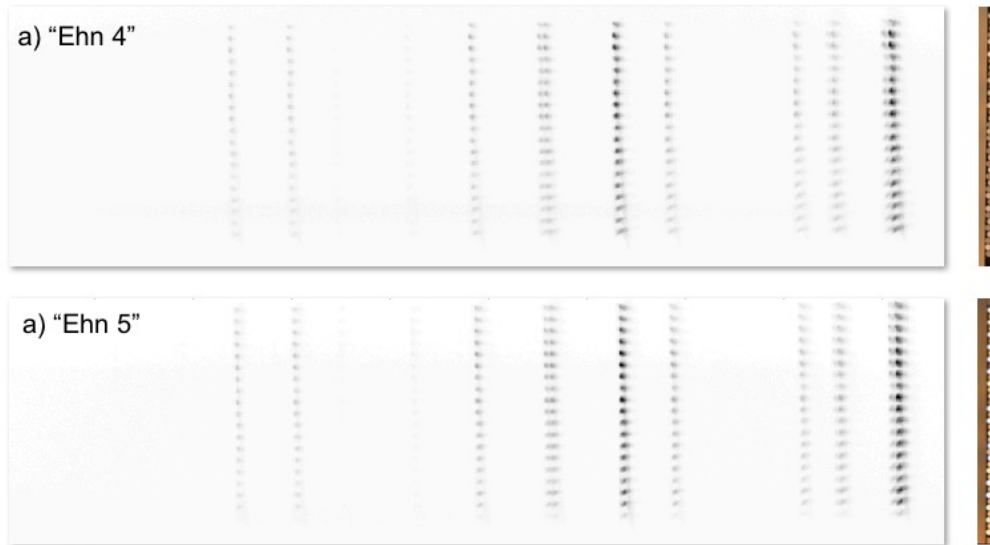


Figure 16: The raw images of the two fibers from Argon emission spectra.

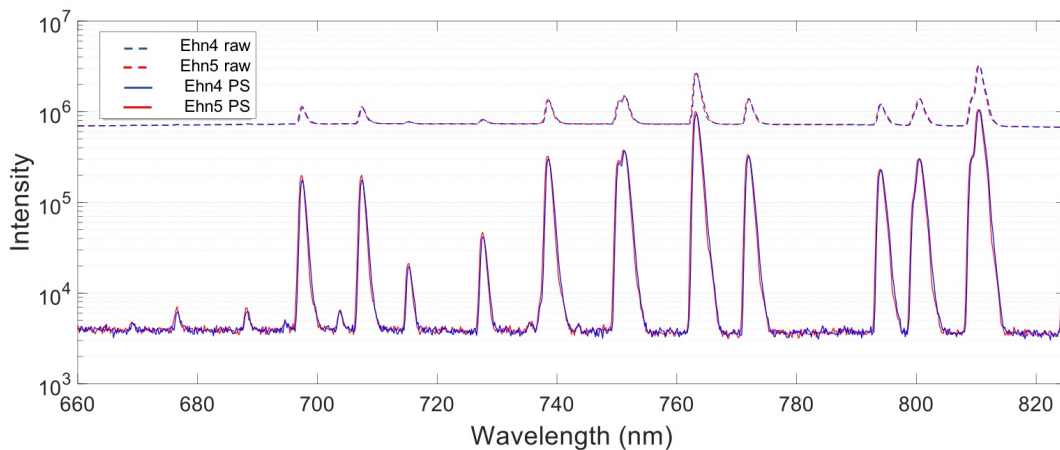


Figure 17: The raw and PS Argon emission spectra of the two fibers).

The results illustrate that the spectra lines achieved by using the two fibers have an almost perfect overlap, which means that although these fibers are handmade, the individual differences between these two are considered negligible. The PS performance further shows that stray light is evidently reduced, which shows the fibers' ability to apply PS method. This first testing result shows the production replicability and the capability for stray light suppression of the fibers, at the same time, lay the foundation for the feasibility of the subsequent experiment.

**Comparison among the optical fibers inside the customized fibers** In order to determine the properties of the single fibers inside the customized fibers, the spectra of

three single optical fibers at different position in “Ehn 5” a) b) c) in Fig. 18) were picked and analyzed. In detail, the PS method was applied to the complete image, then three spectra from the positions at the top, middle and bottom were extracted and compared to each other.

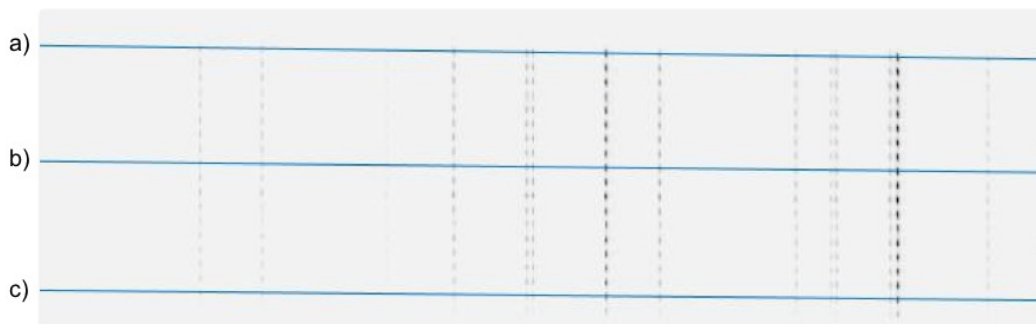


Figure 18: The raw image of the fiber and the position choices of the three fibers (Note that a) and c) are located on the border while b) is in the middle).

As can be seen in Fig. 19 and 20, the background values of the spectra are lower from the two single optical fibers on the border (top and bottom) than the one in the middle. It could be explained by the stronger stray light contribution in the middle fiber compared to those in the fibers on the border. It has to be noted that the fibers on the border of the output end are located also on the border of the collection end, as well as the fiber in the middle.

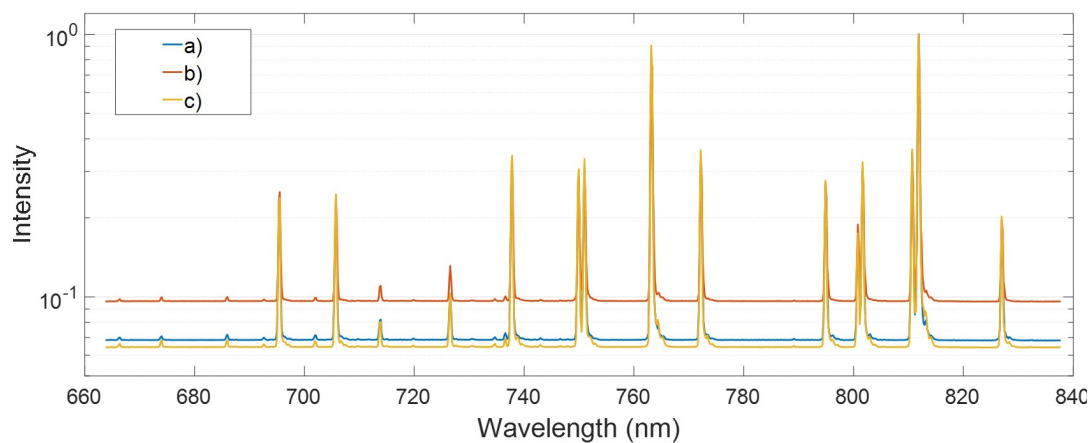


Figure 19: The raw Argon emission spectra at the three positions a), b) and c).

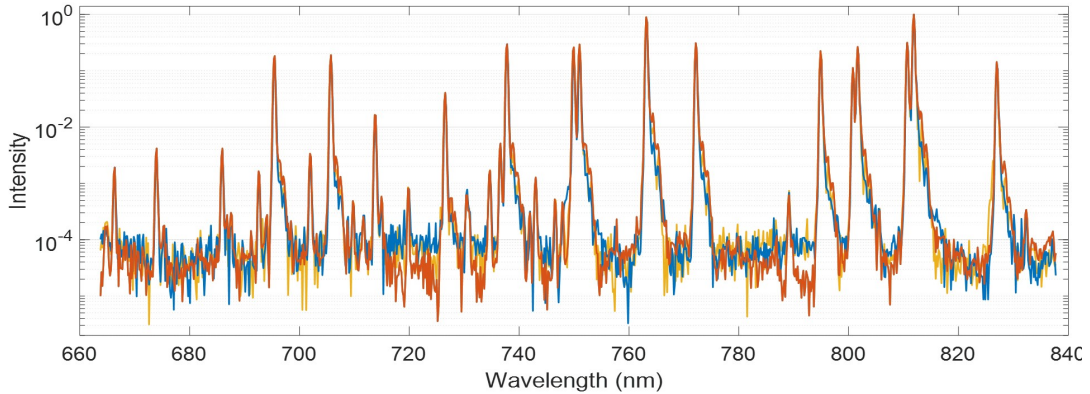


Figure 20: The PS Argon emission spectra of the three positions a), b) and c).

The single optical fibers in the middle have stray light contributions from  $360^\circ$ , meanwhile the fibers on the border have only contributions from one side ( $180^\circ$ ). On the contrary, after the PS process, the difference in the background values is eliminated. All three spectra have the same level amount of background signals. It indicates that the single optical fibers are capable of containing the full frequency information from the light source. Also, it gives further evidence that the customized fibers are capable of applying PS method.

### 5.1.2 Comparison between different imaging magnifications

The single fibers inside the customized fibers have circular side sections, each with a diameter of about  $120\mu\text{m}$  (appendix A) which gives the output end with a width of about  $120\mu\text{m}$ . The relative size (width) relation between the entrance slit and the fibers affects the light usage and properties of the light modulation. This relation can be adjusted either by changing the imaging magnifications of the fibers on the slit, by adjusting the slit width. However, spatial resolution can be influenced by different imaging magnifications but not by using different slit width. Therefore, the relative size (width) relation between the entrance slit and the fibers were experimentally investigated. Magnifications of 1:1, 1:2, 1:4 were tested on both two fibers “Ehn-4” and “Ehn-5”. For simplification, the displayed results are all from fiber “Ehn-5”. Also, the acquisition setup and opening size of the aperture were adjusted to achieve the best imaging quality.

Fig. 21 shows the relative size relations between different magnifications of fibers with fixed-size slit. As can be seen by observation, in principle, the light utilization increases by the decrease of magnification when the image size of the fibers is larger than the slit. The result of raw and PS Argon emission spectra of 1:1, 1:2 and 1:4 magnification are shown in Fig. 22, 23 and 24. Acquisition settings of three magnifications are respectively:  $6000 \times 0.05\text{s}$  (1:1);  $6000 \times 0.07\text{s}$  (1:2);  $6000 \times 0.15\text{s}$  (1:4).

From direct observation from the spectra, the reduction of stray light has a rising trend when magnification reduces ( $1:1 < 1:2 < 1:4$ ), which is in consistence with the previous conjecture. However, with 1:4 magnification, the shape of the spectral peaks is

less symmetric than of the other two cases. Also, it appears to have worse background and light loss, since the acquisition time is been doubled to achieve the same amount of light as with 1:2 magnification. The loss of light is most probably due to the long distance between the fiber and the collection end (in 1:4 magnification, distance between fiber output end and entrance slit was about 120cm). Longer traveling distance of light in the focusing system leads to wider light spread and less light is collected by the focusing lens.

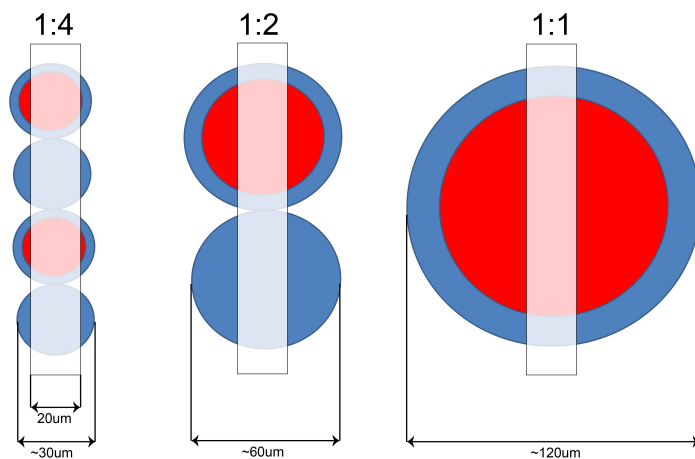


Figure 21: The sketch of different magnifications of the fiber (collection end) as it is imaged onto the entrance slit of the spectrometer. The white translucent rectangles represent the entrance slit with fixed-size ( $20\ \mu\text{m}$ ) while the circles represent the fiber images with different magnifications.

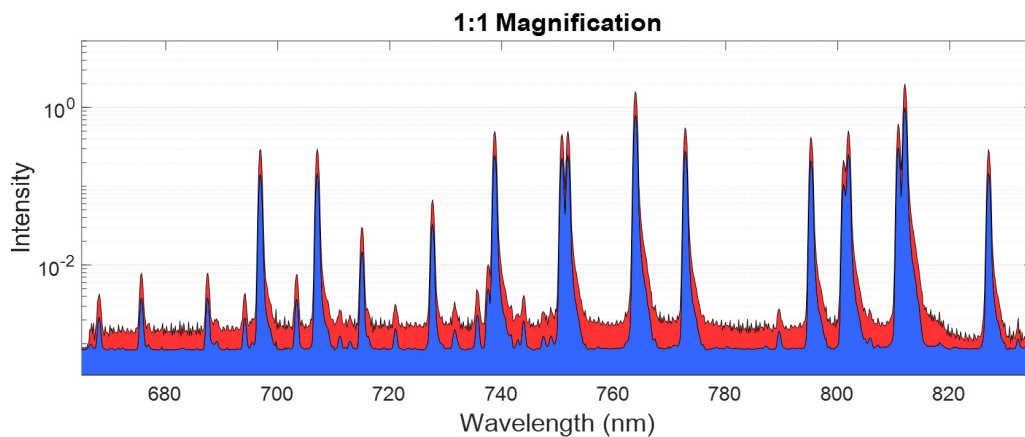


Figure 22: The raw and PS Argon emission spectra and raw image of 1:1 magnification.

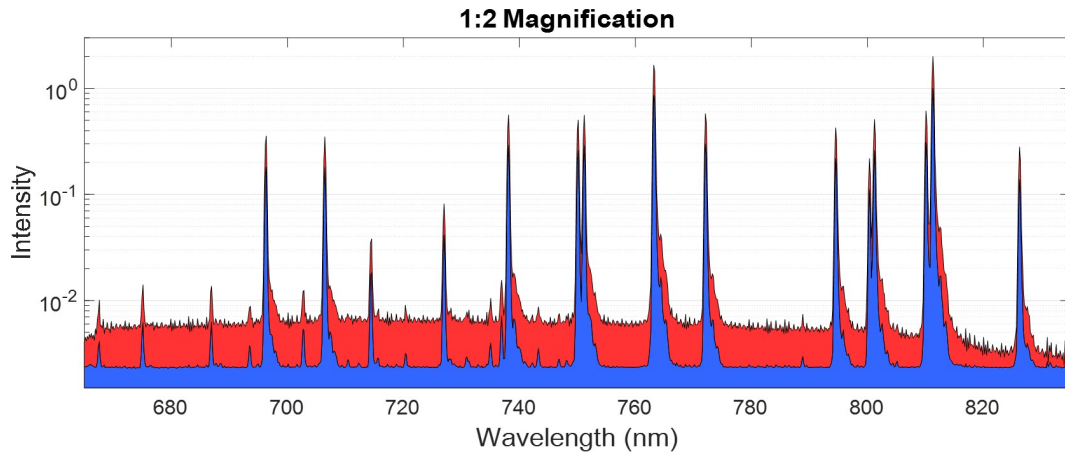


Figure 23: The raw and PS Argon emission spectra and raw image of 1:2 magnification.

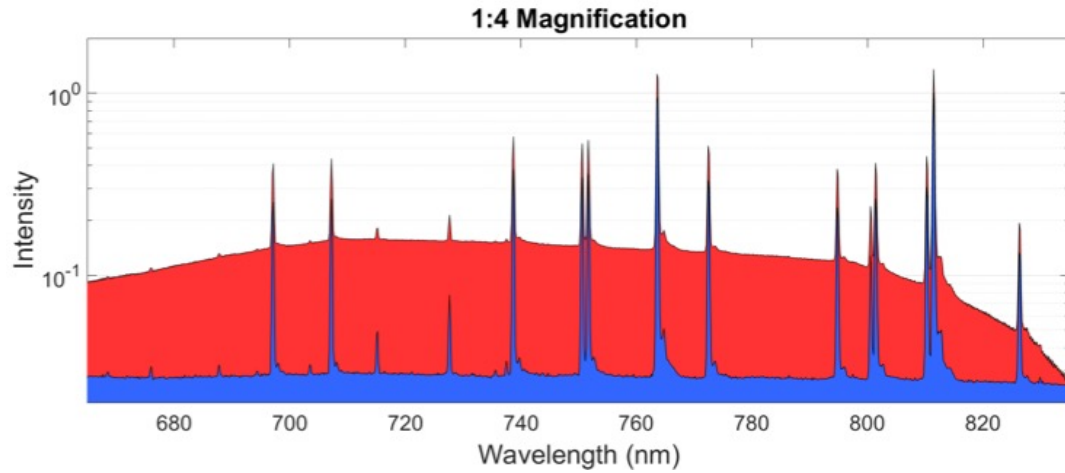


Figure 24: The raw and PS Argon emission spectra and raw image of 1:4 magnification.

In addition, the focusing system becomes fairly sensitive with such long focusing distance. A slight disturbance to the system could vary the image of the fibers focusing on the entrance slit, causing the severe distortion. Therefore longer acquisition time is needed, which could result in another problem - lower signal-to-background values. In terms of both aspects and to find a balance between them, 1:2 magnification is considered the most balanced setup for the present system and chosen for the rest experiment. It should, however, be noted that the PS algorithm is able to efficiently remove the additional background that is seen with the 1:4 magnification.

## 5.2 A Demonstration of Fiber-based PS Technique in Emission

In emission spectra, intensive lines rise the stray light level nearby and obscure the lower spectral peaks.

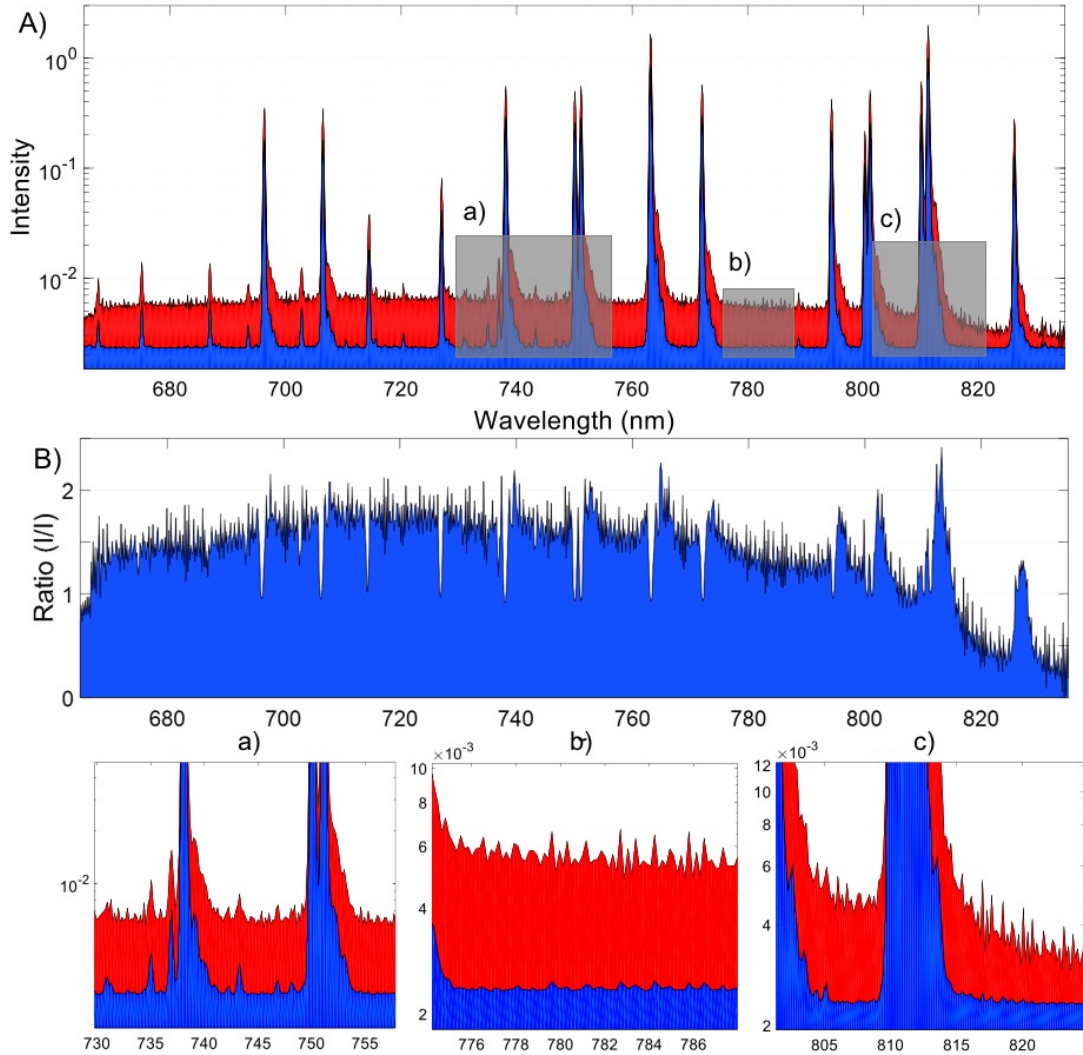


Figure 25: The raw and PS spectra from an Argon emission lamp. A) The spectra in logarithmic scale; B) the intensity ratio between raw and PS spectrum; a) and c) are two typical examples of the wings on strong emission peaks conceals the weak spectral lines; b) shows reduction of noise-like signals by PS.

The Argon emission spectra from an Argon emission lamp are shown in Fig. 25 A) with and without PS analysis. The ratio between the raw data and PS spectrum is shown in Fig. 25 B) and three partially zoomed-in figures of the spectra are shown in Fig. 25 a), b) and c). The normalised spectra are shown in logarithmic scale. Background data were acquired by blank recordings and background subtraction was applied to all spectra.

As shown in Fig. 25 A), the raw spectrum appears to have higher levels of background, whereas the background signal level is significantly reduced in the PS spectrum. Also, the white noise feature of the background signals is reduced. Fig. 25 B) shows that the background is reduced stably across the wavelength of the spectrum. The factor is up to 3 in some regions. In Fig. 25 a) and c), superposition of wings of strong emission



lines conceal weak spectral in the local region in the raw spectrum that are revealed in the PS spectrum. Stray light reduction by PS is particularly obvious in Fig. 25 c) where the baseline is flat in the PS spectrum whereas the raw spectrum shows gradient close to strong spectral peaks due to stray light. Though the performance in stray light suppression is effective, light reduction in signal lines also takes place. In Fig. 25 b), it shows that reduction in background is also obvious. The standard deviation is calculated by smoothing the spectra of wavelength region from 774 nm to 768 nm and it is reduced to a factor more than 5 from the raw spectrum to PS spectrum. Especially in the emission spectrum, the background reduction is rather efficient.

### 5.3 Fiber-based Laser Raman Spectroscopy

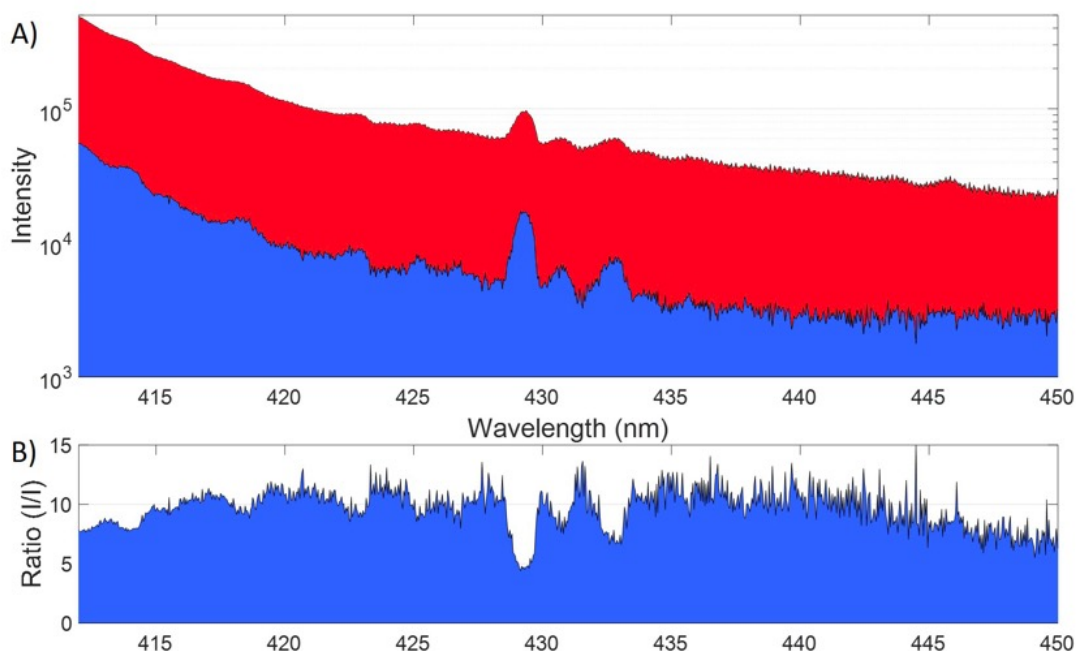


Figure 26: The raw and PS Raman spectra of solid phase naphthalene. A) is the spectra in logarithmic scale; B) is the intensity ratio between raw and PS spectrum.

Laser Raman spectroscopy is often affected by stray light due to intense elastic scattering, including Rayleigh scattering and reflection. It generally appears as an expanding, strong wing in the Raman scattering region. In Fig.26, the raw and PS Raman spectra of naphthalene are shown.

As seen in the spectra, the transition near the laser wavelength of 405 nm is almost covered by the wing in the raw spectrum, while it becomes clearer in the PS spectrum, which means there is possibility of studying the spectral features near the laser wavelength. Also, in the region near 445 nm, two peaks of background signals possibly from the environment are recognised and eliminated by the PS processing. But there is obvious reduction of the

signal peaks which results in a problem from multiple sources. One of the possible reason is that the camera loses contrast of signal and background when the light is relatively strong. In the setup, there was no standard mounting for the connection between the camera and the spectrometer, so a homemade mounting was built. This homemade mounting was flexible and simple indeed, however, the gap between the camera and spectrometer may cause leakage from outside and be responsible for the contrast reduction in the acquired spectra. Another possible reason is that the modulated signal created by the fibers is more sin-like instead of a square pulse comparing to the grid. This could lead to that more signal appear in the first order in the Fourier frequency domain, which, in principle, would improve spectral contrast.

## 6 Conclusion

In conclusion, this thesis work established a feasible fiber-based suppression method for stray light, which is demonstrated by experimental study of emission from Argon atoms and Raman spectroscopy. The principle of the method is to combine the customized fibers with the PS method, creating a predefined pattern of light with a certain periodicity while inserting the signal into the spectrometer. Stray light can be distinguished and separated from the signal light due to their different spatial characteristics. Further than that, it is able to reduce background and high-frequency noise-like signals as well. In addition, the introduction of the customized fiber also allows more flexibility in the experimental setup and is a low-cost, convenient method with potential to be further studied.

## 7 Outlook

There are several research directions available in future studies from this project. Firstly, more testings can be done in order to achieve higher experimental diversity of this method. Different spectroscopic methods, for example, absorption can be studied. Different concepts of experimental setups can be built and experimentally tested. Better equipment can be used, including spectrometer with longer focal length and camera with higher sensitivity and lower noise.

Secondly, the fiber design can be further improved. As the testing of different magnification shown in section 5.1.1, fiber with smaller size could be beneficial for light collection. If the fiber diameter is made smaller than the entrance slit, in principle it can be directly imaged onto the slit plane with 100% light usage and no focusing system is needed anymore. Additionally, the fiber length can be made longer so that the light source system can be relatively independent from the detection system in order to introduce more experimental flexibility.

Finally, consider a future product, an integrated spectroscopic system with the fiber included that can be designed. Comparing to the existing stray light suppression spectrometers, this inexpensive and experimentally-easy method could have its advantages.

## Acknowledgement

The ÅForsk Foundation (grant no. 13-369) is acknowledged for their financial support.

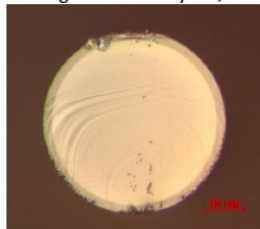
## References

- [1] J Michael Hollas. *Modern spectroscopy*. John Wiley & Sons, 2004.
- [2] Ewen Smith and Geoffrey Dent. *Modern Raman spectroscopy: a practical approach*. John Wiley & Sons, 2013.
- [3] R Donaldson. Stray light in monochromators. *Journal of Scientific Instruments*, 29(5):150, 1952.
- [4] Elias Kristensson, Joakim Bood, Marcus Alden, Emil Nordström, Jiajian Zhu, Sven Huldt, Per-Erik Bengtsson, Hampus Nilsson, Edouard Berrocal, and Andreas Ehn. Stray light suppression in spectroscopy using periodic shadowing. *Opt. Express*, 22(7):7711–7721, Apr 2014.
- [5] Paul A Remillard and Michael C Amorelli. Lock-in amplifier, May 11 1993. US Patent 5,210,484.
- [6] Mark AA Neil, Rimas Juškaitis, and Tony Wilson. Method of obtaining optical sectioning by using structured light in a conventional microscope. *Optics letters*, 22(24):1905–1907, 1997.
- [7] Elias Kristensson and Andreas Ehn. Improved spectral sensitivity by combining periodic shadowing and high dynamic range imaging. *Spectroscopy Letters*, 49(2):91–95, 2016.
- [8] Richard E Poulson. Test methods in spectrophotometry: Stray-light determination. *Applied Optics*, 3(1):99–104, 1964.
- [9] Daryl E Freeman and Ian G Ross. The planar vibrations of naphthalene. *Spectrochimica Acta*, 16(11-12):1393–1408, 1960.
- [10] Wolfgang Demtröder. *Laser spectroscopy: basic concepts and instrumentation*. Springer Science & Business Media, 2013.
- [11] Al H Cherin. *An Introduction To Optical Fibers*. Japan, 1983.
- [12] Andor. Andor shamrock 303 specifications. Website, 2010. [http://www.andor.com/pdfs/specifications/Andor\\_Shamrock\\_303\\_Specifications.pdf](http://www.andor.com/pdfs/specifications/Andor_Shamrock_303_Specifications.pdf).
- [13] Andor. Andor luca r604 emccd. Website, 2010. [\textbf{http://www.andor.com/pdfs/specifications/Andor\\_Luca-R\\_604\\_Specifications.pdf}](http://www.andor.com/pdfs/specifications/Andor_Luca-R_604_Specifications.pdf).
- [14] Elias Kristensson, Andreas Ehn, and Edouard Berrocal. High dynamic spectroscopy using a digital micromirror device and periodic shadowing. *Optics Express*, 25(1):212–222, 2017.

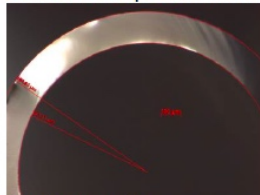
## A Parameters of the Customized Fibers (from the manufacturing research group)

19x circular-structure to 37(19x) line structure

- fiber:
  - Preform Heraeus SWU 1.1 core /clad ratio 1/1,1 → fiber core 114 $\mu\text{m}$ ; cladding 126 $\mu\text{m}$  NA0,22 $\pm$ 0,02
  - Coating Standard-Acrylate; diameter  $\sim$ 230 $\mu\text{m}$



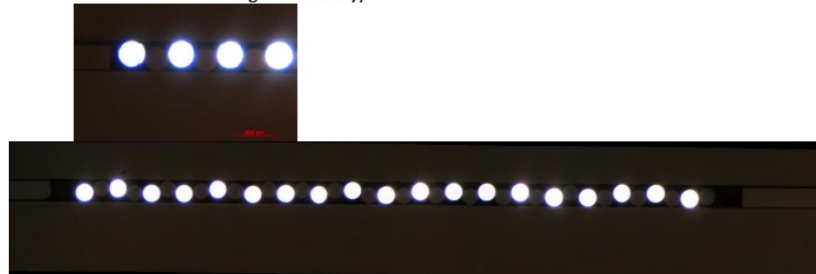
- capillary for circular side
  - Material : F300
  - Dimension untapered: outer diameter:  $\sim$ 1610 $\mu\text{m}$ /inner diameter  $\sim$ 1294 $\mu\text{m}$



- material for the line side
  - "distance" fiber: equal to the guidance fiber
  - Distance holder: microscope plate
  - substrate: BK7, we are not able to make the dimensions of the block smaller because of the hand polish of the 37 fibers in a line after arranging all.

Arrangement of fibers in line

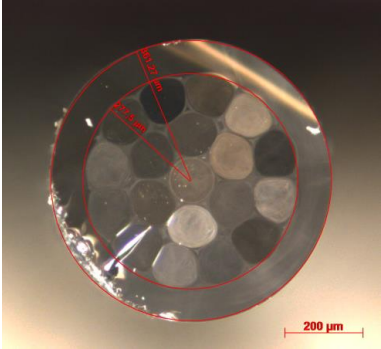
- put the central fiber of the bundle in the middle of the linear arrangement,
- put the surrounding 6 fibers of the bundle next to the first fiber (3 on each side)
- put the remaining 12 fibers of the outer ring on the outside of the linear arrangement (6 on each side)
- between 2 guidance fibers lies a "distance" fiber  
coupling light in from the bundle side; line side in the microscope ( for the stitching pic small amount of reflected light necessary)



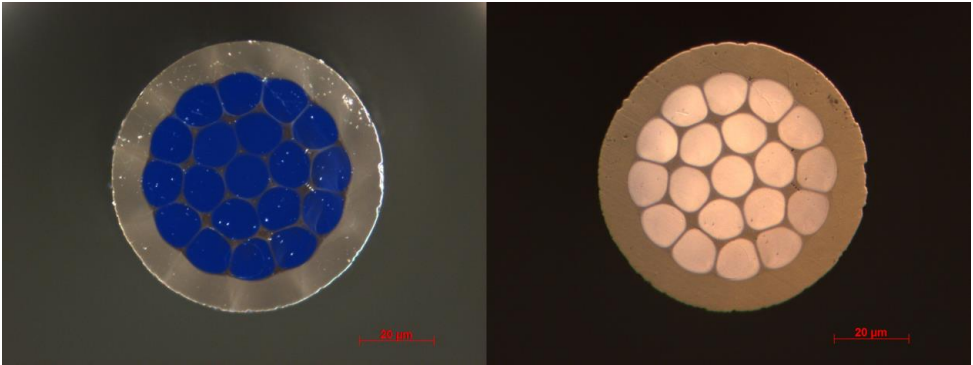
Ehn-2

Circular side:

Dimensions: outer dimensions ~724μm, fiber circle ~554μm

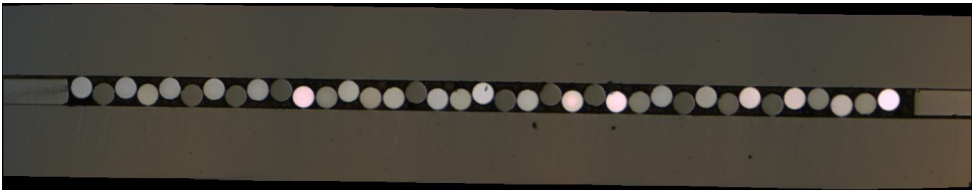


cleaved by hand



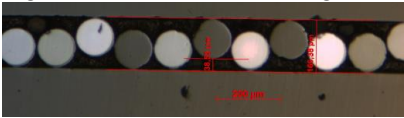
Polished circular side

Line side (reflected light)



Distance in height ~40μm

- 7 guidance fibers with a max. height difference from ~40μm; ratio 12/7

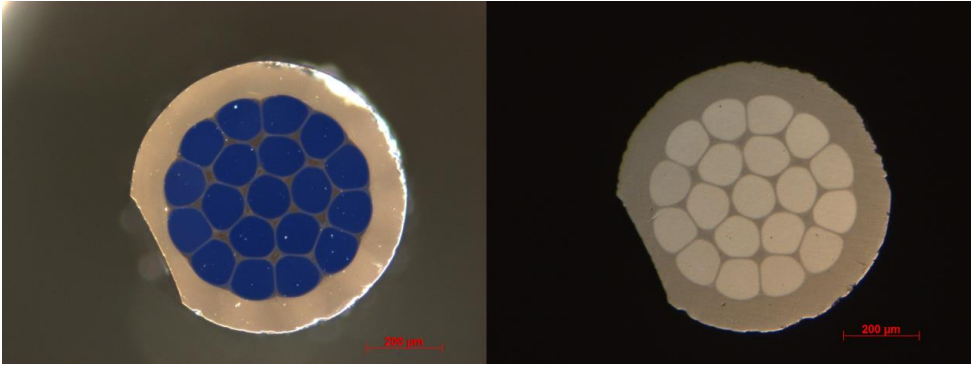


Ehn-4

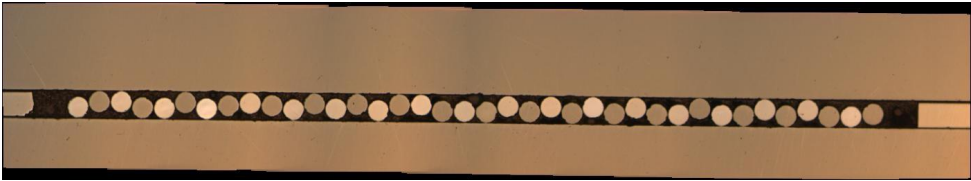
Circular side:

Dimensions: outer dimensions 724μm, fiber circle 554μm

Polished circular side

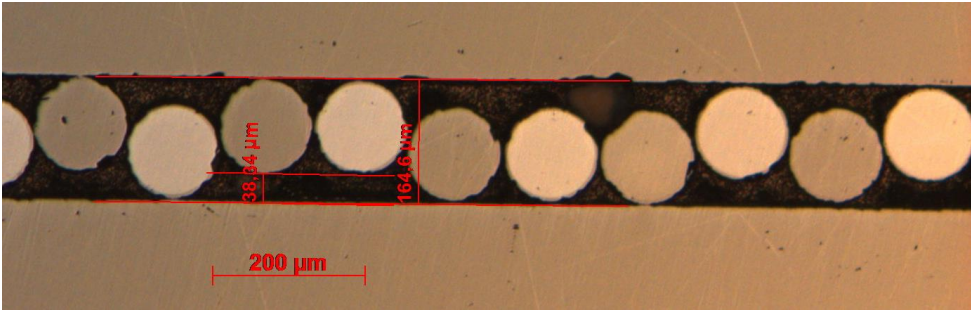


Line side (reflected light)



Distance in height ~40μm

- 7 guidance fibers with a max. height difference from ~40μm; ratio 10/9

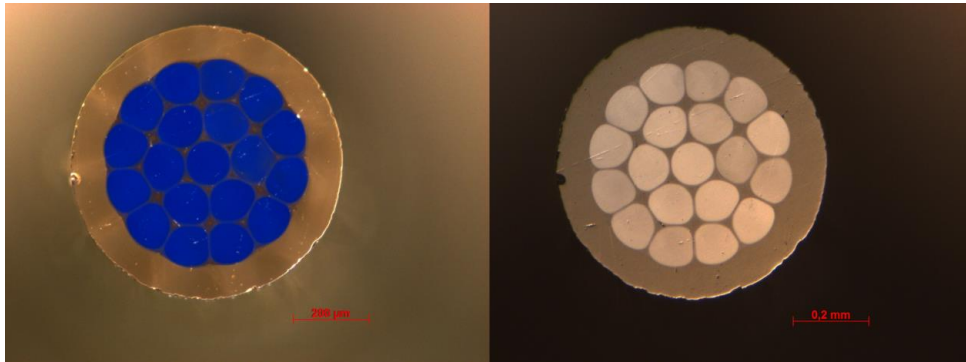


Ehn-5

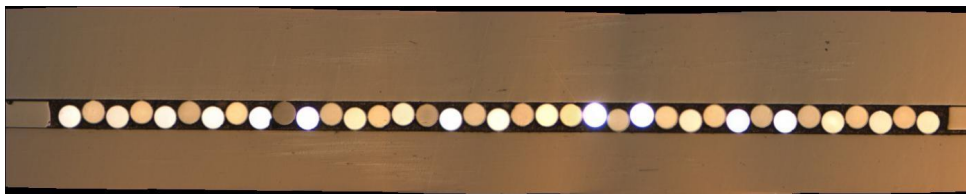
Circular side:

Dimensions: outer dimensions  $\sim 724\mu\text{m}$ , fiber circle  $\sim 554\mu\text{m}$

Polished circular side

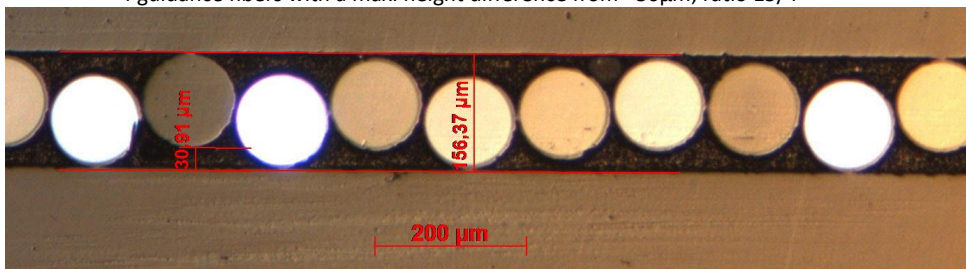


Line side (reflected light)



Distance in height  $\sim 31\mu\text{m}$

- 4 guidance fibers with a max. height difference from  $\sim 30\mu\text{m}$ ; ratio 15/4





## B More sketches of Experimental Setup

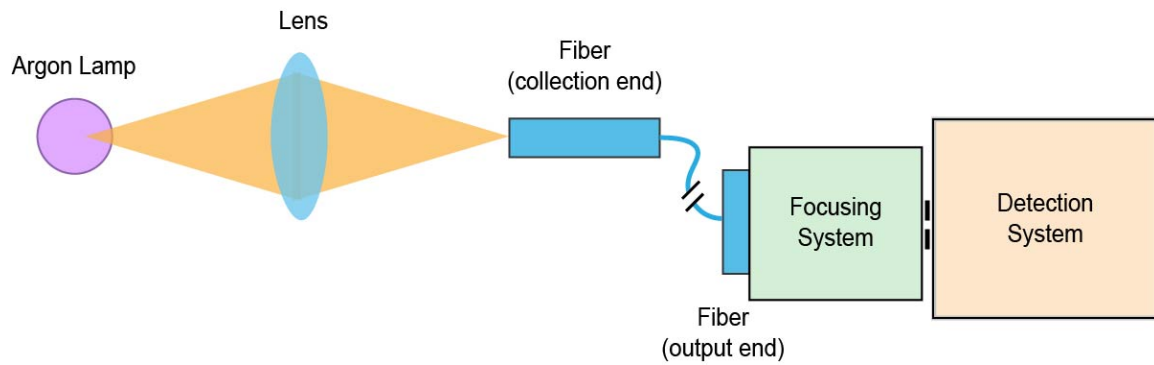


Figure 27

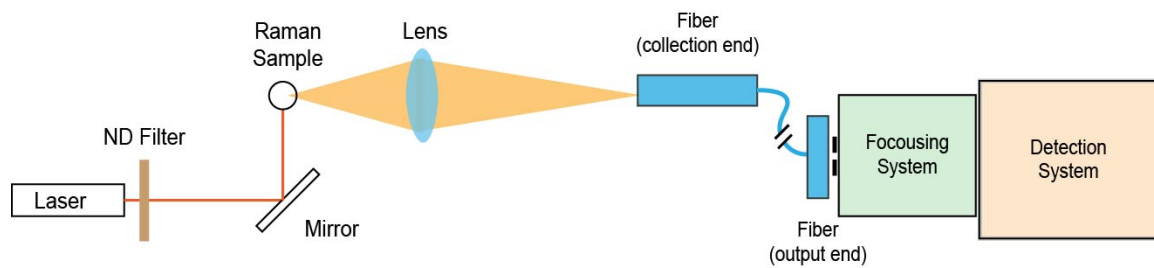


Figure 28

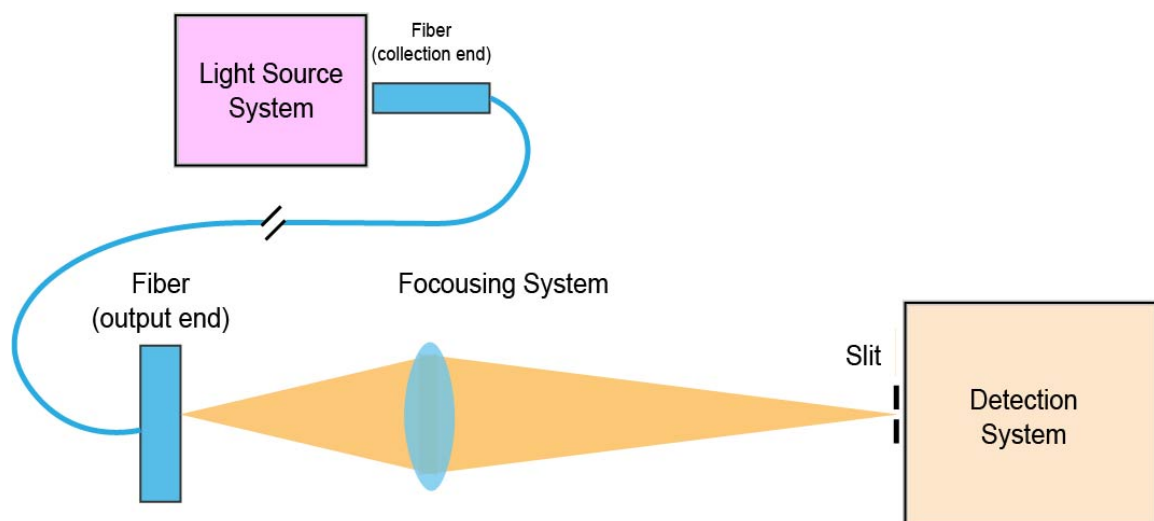


Figure 29

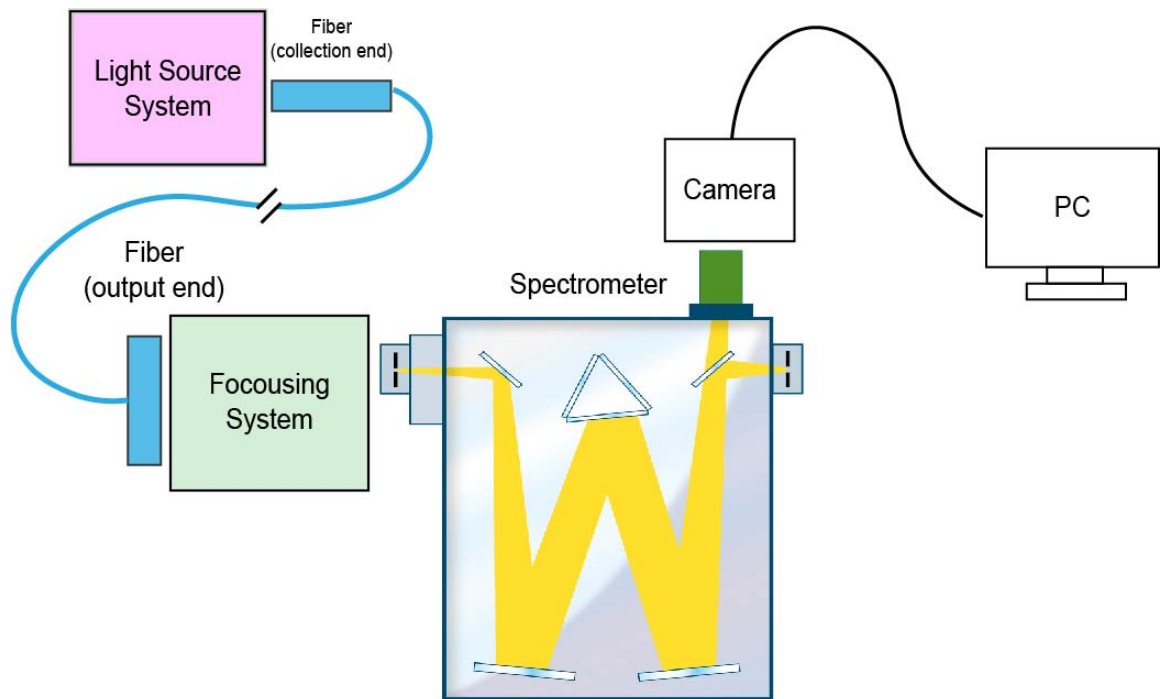
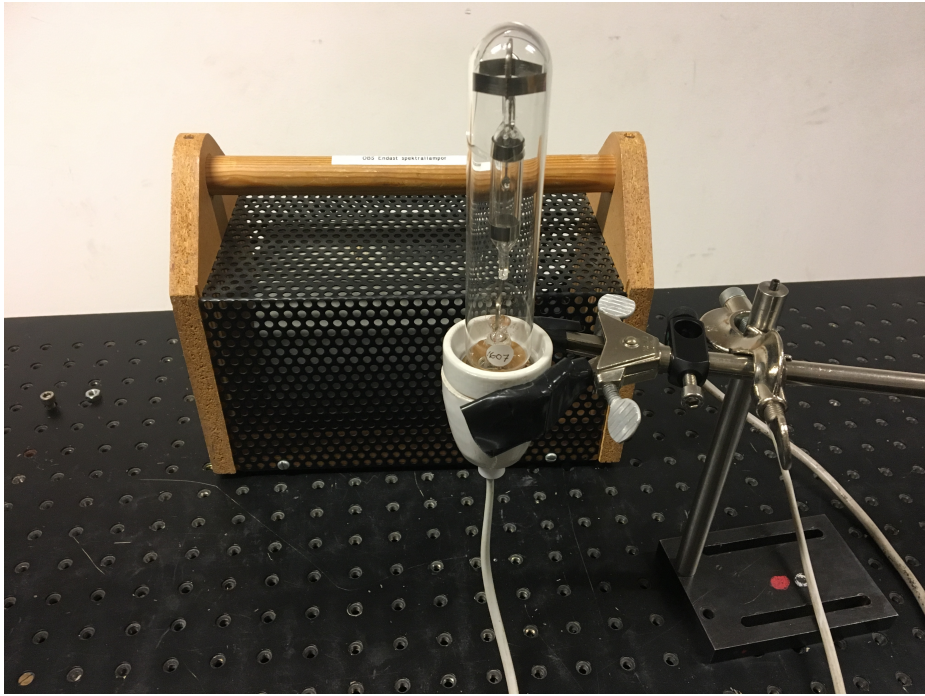


Figure 30



Figure 31



*Figure 32*